Heliyon 10 (2024) e39090

Contents lists available at ScienceDirect

Heliyon

journal homepage: www.cell.com/heliyon

Research article

Nitrogen functionalized biomass derived mesoporous carbon nanomaterials for electrochemical detection of lead (II) ions

Ritika Sharma [a], Dharmender Singh Rana [b], Abhishek Awasthi [c], Dilbag Singh [a,*], Ahmed A. Ibrahim [d,e], Ahmad Umar [d,e,f,**], Sotirios Baskoutas [g]

[a] Department of Environmental Sciences, Central University of Himachal Pradesh, Dharamshala, 176215, HP, India
[b] Department of Physics, MLSM College Sunder Nagar, Chaterokhri, Mandi, HP, India
[c] Department of Biotechnology, School of Basic and Applied Sciences, Maharaja Agrasen University, Baddi, 174103, HP, India
[d] Department of Chemistry, Faculty of Science and Arts, and Promising Centre for Sensors and Electronic Devices (PCSED), Najran University, Najran, 11001, Kingdom of Saudi Arabia
[e] STEM Pioneers Training Lab, Najran University, Najran, 11001, Kingdom of Saudi Arabia
[f] Department of Materials Science and Engineering, The Ohio State University, Columbus, OH, 43210, USA
[g] Department of Materials Science, University of Patras, 26504, Patras, Greece

ARTICLE INFO

Keywords:
Coconut husk
Nitrogen functionalized mesoporous carbon
Cyclic voltammetry
Lead (II) ions

ABSTRACT

This study has explored the sustainable solution after designing an economical metal-free biomass-derived nanocarbon for the selective sensing of lead. The nitrogen and sulfur-rich mesoporous nanocarbon is designed through a facile hydrothermal-assisted thermal annealing method. The high-temperature treatment gave nanocarbon unique carbon dot decorated layered morphology, while nitrogen and sulfur precursor thiourea and melamine strengthened the nanomaterial stability, sensitivity, and selectivity toward lead metal ions. The high specific surface area of mesoporous nanocarbon viz., 1671.93 m^2/g with the pore width and pore volume of 2.02 nm and 0.476 cm^3/g has enhanced the conductivity of as-synthesized sensor, which helps in increasing sensitivity toward lead. The high conductivity was also confirmed through cyclic voltammetry, where an 80 % increment in current was observed in the case of the modified electrode when compared with bare GCE. The differential pulse normal voltammetry and differential pulse anodic stripping voltammetry were performed to calculate the detection limit, where an excellent detection limit of 22 nM was obtained from the DPASV technique. Moreover, the nanomaterial was also tested for detecting lead in tap water. The as-synthesized nanocomposite is highly efficient and selective for the detection of lead. This study will motivate the researchers to engineer sustainable and efficient devices for sensing metal pollutants.

1. Introduction

The persistent demand for lead (Pb) in various industrial and consumer products poses a significant challenge to environmental quality and human well-being. Lead is one of the most toxic heavy elements that accumulate in the environment due to its non-

* Corresponding author. Department of Environmental Sciences, Central University of Himachal Pradesh, Dharamshala, 176215, HP, India.
** Corresponding author. Department of Chemistry, Faculty of Science and Arts, and Promising Centre for Sensors and Electronic Devices (PCSED), Najran University, Najran, 11001, Kingdom of Saudi Arabia.
E-mail addresses: dilbagrana@hpcu.ac.in (D. Singh), ahmadumar786@gmail.com (A. Umar).

https://doi.org/10.1016/j.heliyon.2024.e39090
Received 14 June 2024; Received in revised form 15 September 2024; Accepted 7 October 2024
Available online 11 October 2024

biodegradable nature. The contamination occurs as lead leaches into soil and water sources, where plants and aquatic organisms subsequently absorb it. It eventually makes its way up the food chain to affect human and animal populations. Human functions are also affected by lead toxicity. According to the United States Center for Disease Control and Prevention and the World Health Organization, a blood lead level of 10 μg/dL or above is of serious concern; even a lower level may lead to harmful health effects and there is no known safe exposure level. The common adverse health effects of lead concentration in the human body are neurological and organ impairments. Therefore, it is crucial to monitor the lead flow in waste however, its detection at open sources such as rivers, ponds, and seas is still a major challenge. Therefore, an industrial-based sensor for monitoring lead leakage at its point sources is the need of the hour. Despite the pressing need, most of the previously reported sensors, such as metal-organic frameworks (MOFs) [1], DNA-mediated sensors [2,3], metal-based nanocomposite [4–10], transition metal dichalcogenides [11,12] and molecularly imprinted polymers (MIPs) [13,14], often suffer from complexity associated with their synthesis procedure, interaction mechanism, sensing stability, high cost, and toxicity of waste generated from metal ions. This discourages their commercialization [15] and motivates the researchers to explore sustainable and highly efficient sensors that can meet the requirements of commercialization [16].

Carbon-based nanomaterials are among the best alternatives for costly and complicated metal-based sensors due to their high conductivity and specific surface area. Moreover, the abundance of carbon makes it an economical and sustainable nanomaterial [17]. The functionalization of carbon-based nanomaterial has also been reported to enhance its catalytic and electrochemical applications [18–22]. The widespread applications of heteroatom-doped/functionalized carbon-based nanomaterial in adsorption [23, 24], sensing [25], supercapacitor [26], carbon sequestration [27], and hydrogen evolution reaction [28] underscore its potential and versatility. The synthetic routes reported in the literature for synthesizing carbon-based nanomaterial are mechanical or chemical exfoliation of graphite [29] pyrolysis and chemical activation of biomass. The pyrolysis or carbonization of biomass for extraction of carbon rich material is a new method that is not only gaining wide attention among researchers but also offers easy synthesis, cost-effectiveness and sustainability.

Biomass-derived nanocarbon offers several advantages such as abundance, renewability, sustainability, high specific surface area, easy tunability, biocompatibility and natural heteroatom functionalities [30]. Moreover, the use of biomass waste promotes environmental cleaning and waste management practices. The wide applicability of biomass-derived carbon in fuel cells, electrocatalytic oxidation-reduction reactions, water splitting, hydrogen evolution reactions, supercapacitors, lithium-ion batteries, and sensing makes it more demanding in today's world [25,30,31]. The applicability of biomass-based sensors for lead ions is reported in previous literature. Zeinu et al. have synthesized the composite of biomass-derived carbon and bismuth, and the obtained detection limit was 1.72 pM [32]. Zhu et al., have designed the electrochemical sensor Bi@BAC for lead from *Platanus* seeds. The detection limit obtained in the case was 0.13 μg/L [33]. Chen et al., have coated the bismuth nanoparticles on to the hierarchical porous tubular biochar and the obtained detection limit of the resultant nanocomposite was 0.02 μg/L [34]. Zeng et al., have prepared the ordered mesoporous carbon doped hollow spherical bismuth oxide nanocomposite as an electrochemical sensor for lead ion and the obtained detection limit was 0.025 nM [35]. Agustini et al., have anchored the bismuth nanoparticles on to the biochar for detection of lead and the obtained detection limit was 1.41 nM [36]. Jin et al., have used porous carbon derived from soyabean straw to load platinum nanoparticles and the obtained detection limit from composite was 18 pM [37]. Although bismuth and platinum-decorated biomass-derived carbon offer many advantages regarding excellent detection limit and high sensitivity, its cost and associated toxicity discourage its long-term or commercial uses. Dali et al. have functionalized the biomass with SWCNT, and although the study has obtained an excellent detection limit of 0.01 μM, the complexity and cost associated with the SWCNT limit its further applications [38]. In the study by Xu et al., for nitrogen functionalization milk is used [39]. As milk is edible and used as a dietary product, its use as a nitrogen precursor questions the sustainability agendas. The chemical activation approaches with excellent detection limits for the development of sensors were also achieved by Oliveira and Guan [40,41]. Chemical activation methods suffer from some limitations, such as toxicity associated with the use of high quantities of chemicals, structural stability, and impurities, as the chances of obtaining pure carbon are less in these cases. Thermal annealing methods are also advantageous over chemical activation for the degree of graphitization, conductivity, and carbon richness of nanocomposite. Metal-free functionalization of biomass-derived carbon often suffers from high detection limits and less sensitivity; little or no study is reported on this.

Motivated by the above facts, the present study has successfully designed a sustainable metal-free biomass-derived sensor from coconut husk. Coconut husk is a prevalent secondary biomass waste, a residue of processed food products [42]. The two-step synthetic approach viz., hydrothermal carbonization followed by pyrolysis, was adopted for developing non-metal functionalized carbon nanomaterial. The mesoporous structure offers numerous advantages, such as high specific surface area, high conductivity and more active sites for functionalization. Mesopores of the nanostructure can be easily engineered for different applications. The functionalization of mesoporous nanostructure was done through hydrothermal carbonization with thiourea and melamine. Hydrothermal carbonization is advantageous for retaining the integrity of organic compounds, which aids in increasing the sensitivity and selectivity of carbon nanomaterial as a sensor. Melamine and thiourea are the cheapest precursors for the source of nitrogen and sulfur. The thiourea is an organosulfur compound with amino and C=S bonds. The C=S bond in thiourea provides active sites for binding, which makes the resultant nanocomposite selective for sensing the analyte. Additionally, melamine is also a triazine ligand with three amino groups. The structure of melamine is helpful in providing stability to the resultant nanoparticles, and it aids in the synthesis of graphitic nitrogen. Both melamine and thiourea make excellent choices for designing sustainable sensors due to their cheap cost, easy availability and chemical stability. The novelty of the study lies in the simplicity of designing a sustainable sensor for the efficient detection of lead.

2. Experimental details

2.1. Chemicals

Coconut husk waste was collected from the local market. Concentrated sulfuric acid (H_2SO_4), with 99.9 % purity, sodium acetate (ACS reagent, >99 %), lead nitrate (ACS reagent, >99 %), mercuric chloride (ACS reagent, >99 %), cadmium chloride (99.99 %), cobalt chloride (ACS reagent, 98 %), sodium chloride (ACS reagent, >99 %), aluminum chloride (reagent grade, 98 %), calcium chloride (ACS reagent, >99 %), potassium chloride (ACS reagent, 99–105 %), nickel chloride (98 %), silver nitrate (ACS reagent, >99 %), iron(II) chloride (98 %), iron(III) chloride (ACS reagent, 97 %), potassium hexacyanoferrate(II) trihydrate (ACS reagent, 98.5–102 %) and potassium hexacyanoferrate(III) ACS reagent, >99 % were bought from Sigma Aldrich. All the chemicals were used as received without any further purification. Distilled water (18.2 MΩ cm) was obtained from Milli-Q Ultrapure Water System.

2.2. Instruments

The geometric structure of nitrogen functionalized nanocarbon is studied through an X-ray diffraction pattern with Cu Kα radiation (λ = 1.54178 Å) on the instrument Rigaku Japan XRD. Field emission scanning electron microscope (FE-SEM) and high-resolution transmission electron microscope (HR-TEM) images were obtained from the instrument Carl Zeiss Model Supra 55 Germany and JEOL JEM 2100, 200 Kev, respectively. The chemical composition and connectivity were obtained through an X-ray photoelectron spectroscopy (XPS) analysis technique using Thermo Fischer Scientific ESCALAB Xi^+. All the electrochemical sensing experiments were performed with the electrochemical workstation, Corrtest CS2350.

2.3. Synthesis of N-rich nanocarbon

The synthesis process of N-rich nanocarbon is a step-wise process. The dried coconut waste was first treated with 50 ml of concentrated sulfuric acid for 24 h to remove the moisture, oxygen-containing functional groups, and other impurities, then after consecutive washing, black carbon powder underwent thermal treatment at 1200 °C under N_2 atmosphere with the flow rate of 0.2 mL/min. This treatment removes the volatile impurities and aids in the synthesis of a pure carbon matrix with a mesoporous structure. Afterward, the resultant carbon powder (200 mg) was mixed with thiourea and melamine in equal proportion, and the mixture was

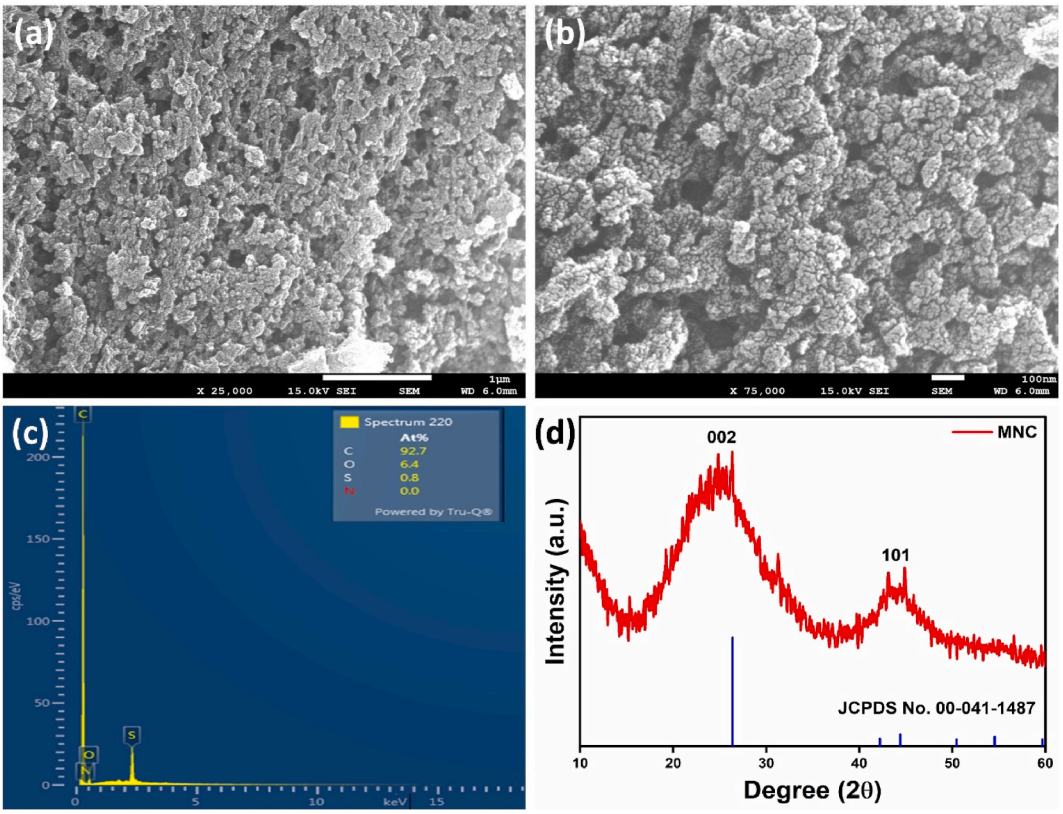

Fig. 1. **(a,b)** Low and high magnification FESEM images, **(c)** EDS and **(d)** XRD of nanocarbon structure.

sonicated in ethanol. The sonicated solution mixture was transferred into a Teflon-lined autoclave. The hydrothermal treatment was given for 6 h at 200 °C. The black mass collected after hydrothermal treatment is then dried in the hot air oven at 70 °C.

2.4. Electrochemical sensing

All the electrochemical sensing experiments were performed using an electrochemical workstation (Corrtest CS2350). The three-electrode setup was prepared, where platinum wire, KCl saturated Ag/AgCl, and glassy carbon electrode (GCE) were used as counter, reference, and working electrode respectively. The slurry of nanomaterial was prepared in DI water (1mg/2 ml). Before modification of the working electrode, it was polished with 0.3 μm alumina powder. After 30 min of sonication, 5 μL slurry is dropped onto the surface of the working electrode and allowed to dry under a 100 W tungsten filament bulb. The dried electrode was then used as a sensor. The electrochemical techniques, viz., cyclic voltammetry, differential pulse normal voltammetry (DPNV) and differential pulse anodic stripping voltammetry (DPASV) are used where 0.1 M acetate buffer of pH 5 is used as an electrolyte.

3. Results and discussion

3.1. Characterizations and properties

The low magnification FE-SEM image (Fig. 1(a)) of mesoporous nanocarbon (MNC) has shown a dense and fluffy porous net-like structure. The detailed examination of the high-magnification image (Fig. 1(b)) illustrates that the entire structure is intricately constructed with dot-like nanostructures. The energy dispersive X-ray spectroscopy (EDS) indicates the prevalence of carbon followed by oxygen, nitrogen and sulfur, with no additional impurities detected within the EDS detection limit, as shown in Fig. 1(c). The XRD spectra of MNC are shown in Fig. 1(d), where two distinguished peaks at 24.8° and 44.1° correspond to 002 and 101 crystal facets [23]. These peaks are assigned to the graphitic plane of the mesoporous nanocarbon structure.

Fig. 2 shows the elemental mapping images of the as-synthesized mesoporous nanocarbon. Fig. 2(a) shows the presence of all the elements in a single image where the differently coloured fluorescent dot represents the presence of C, N, S, and O elements. Fig. 2 (b–e), represents the presence of these atoms individually. It is observed from the EDS map that carbon is abundantly spread in the matrix, followed by oxygen. Nitrogen appears to be sprinkled over the carbon bed, while sulfur patches are a little darker, making the composite nitrogen and sulfur-rich.

Fig. 3(a–f) represents the HR-TEM images of N-nanocarbon at different magnifications. The small fibrous transparent layers of carbon matrix, with round shaped dots, conclude that at high temperatures, a sheet of carbon breaks at some place and the small round shaped sheet accumulates on the surface of thin layers of carbon matrix. This appeared to be a mixture of carbon quantum dots and graphene-like layers of nanocomposite. These dots-like structure plays the role of defects and helps in increasing the conductivity and surface area of the nanostructure. The as-synthesized nanostructure appeared to be a hybrid structure, where small crystalline patches appeared in the amorphous network of the carbon structure.

The XPS spectra of as-synthesized mesoporous nanocarbon have shown the highest amount of carbon, followed by oxygen, nitrogen, and sulfur (Fig. S1). Moreover, Fig. 4(a–d) has shown the deconvoluted spectra of C 1s, O 1s, N 1s and S 2p. The deconvoluted spectra of C 1s have different peaks at locations 284.1, 284.8, 285.6, 286.4, and 287.4 eV, which corresponds to various functional groups present in the nanocarbon viz., C-C (sp^3), C-C (sp^2), C-S, C-N, and C=O respectively. Different functional groups were present due to the nanostructure's addition of thiourea and melamine. In addition to these, the oxygen-containing functional groups, viz., carbonyl and oxides of nitrogen and carbon, are also present and are verified from the XPS spectra of O 1s, where the peaks are located

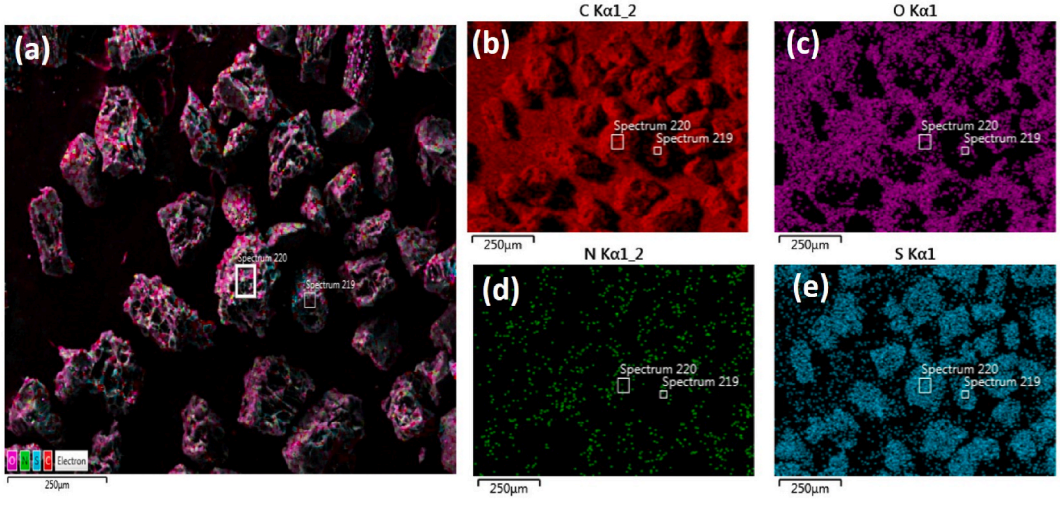

Fig. 2. EDS elemental mapping pattern of **(a)** mesoporous nanocarbon showing the presence of **(b)** C **(c)** O **(d)** N and **(e)** S element.

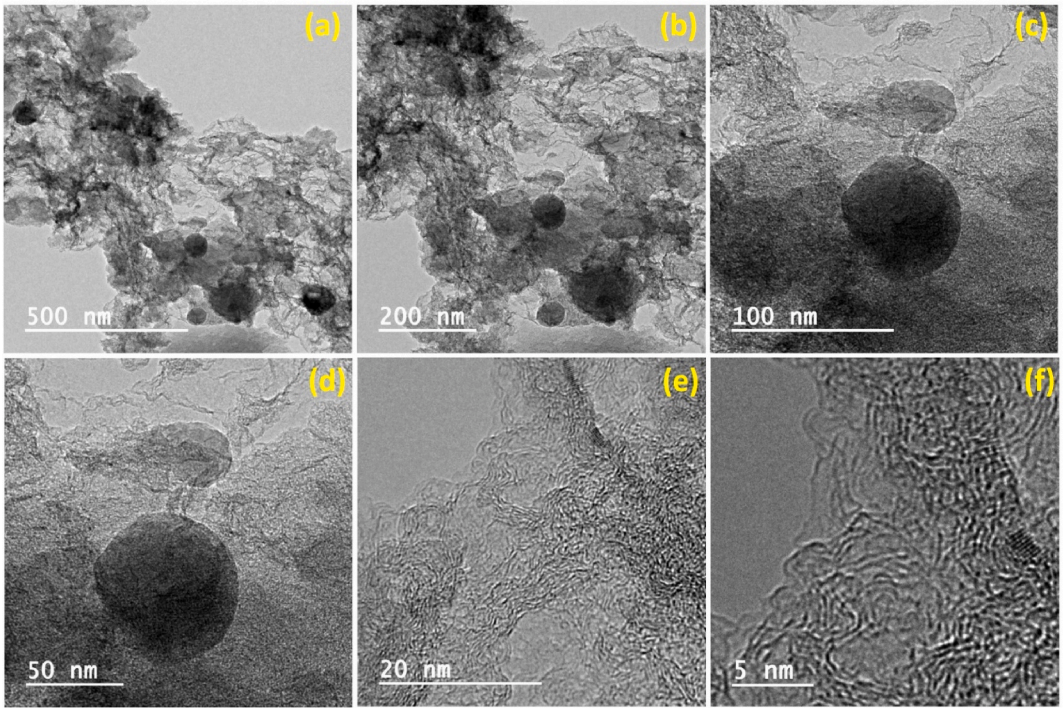

Fig. 3. HR-TEM images of mesoporous nanocarbon at different magnifications viz., (a) 500 nm (b) 200 nm (c) 100 nm (d) 50 nm (e) 20 nm (f) 5 nm.

at 530.7, 532.2 and 533.4 eV. The different bonds of nitrogen viz., -NO_2 (404.9 eV), O=N-C (403.2 eV), -NO (401.8 eV), -NH_2 (400.8 eV), pyrrolic C-NH-C (399.6 eV) and pyridinic C=N-C (398.3eV) bonds represents the diversified richness of N, S in mesoporous nanocarbon. Moreover, sulfur functional groups from thiourea are also indicated in Fig. 4(d), where peaks at 164.1, 165.4167.2 and 168.8 eV represent the R-SH, C-S/S-S, SO_2-C, and C-SO_x functional groups. The XPS data matches the NIST database well. This XPS data is also consistent with the information obtained from EDS.

Fig. 5(a–c) has summarized the Brunauer-Emmett-Teller (BET) study in the form of adsorption-desorption isotherm, pore volume, and pore width, respectively. The nanocarbon has shown the type 1 adsorption isotherm according to IUPAC classification. The obtained surface area of the nanostructure is 1671.93 m^2/g with the pore width and pore volume of 2.02 nm and 0.476 cm^3/g. The obtained pore width of the nanostructure concludes that the nanostructure is mesoporous, while the pore width of nanoparticles appears to be in the range of 2–5 nm. The small range of pore width shows the uniformity in the nanostructure, which is known to increase the catalytic activity and sensing application of the nanostructure. The annealing at high temperatures reduces the pore size, and as the size decreases, the material goes to the nanoscale, due to which surface area increases.

3.2. Electrochemical behavior of mesoporous nanocarbon-modified GCE

Our study compared the electrochemical behavior of the mesoporous nanocarbon-modified electrode with the bare glassy carbon electrode. Fig. 6(a) illustrates the superior performance of the mesoporous nanocarbon-modified GCE in the presence of 10 mM $K_3[Fe(CN)_6]/K_4[Fe(CN)_6]$ in 0.1 M KCl, showing a remarkable ~24 % increase in current, and an even more impressive ~80 % increase in the case of lead. This significant enhancement in conductivity and sensitivity towards lead, attributed to the presence of nitrogen and sulfur-containing functional groups in the nanostructure, not only demonstrates the potential of our research in lead sensing but also in sustainable waste management.

3.2.1. Scan rate study

The scan rate study, a significant research method, was conducted to observe the effect of current with respect to variation in scan speed. This study is instrumental in determining the reaction mechanism and electroactive surface area of the modified GCE. Fig. 7 (a–f) presents the scan rate study of 10 mM $K_3[Fe(CN)_6]/K_4[Fe(CN)_6]$ in 0.1 M KCl and lead. Fig. 7(a) and **(d)** show the current response of bare electrodes with ferroferri, where the current is observed to increase linearly with increased scan rate, indicating that the analyte is freely diffusing in the solvent. The diffusion coefficient value is determined after applying the Randles-Sevcik equation.

$$i_p = 0.44nFAC^o\sqrt{\left(\frac{nFvD_0}{RT}\right)} \quad (1)$$

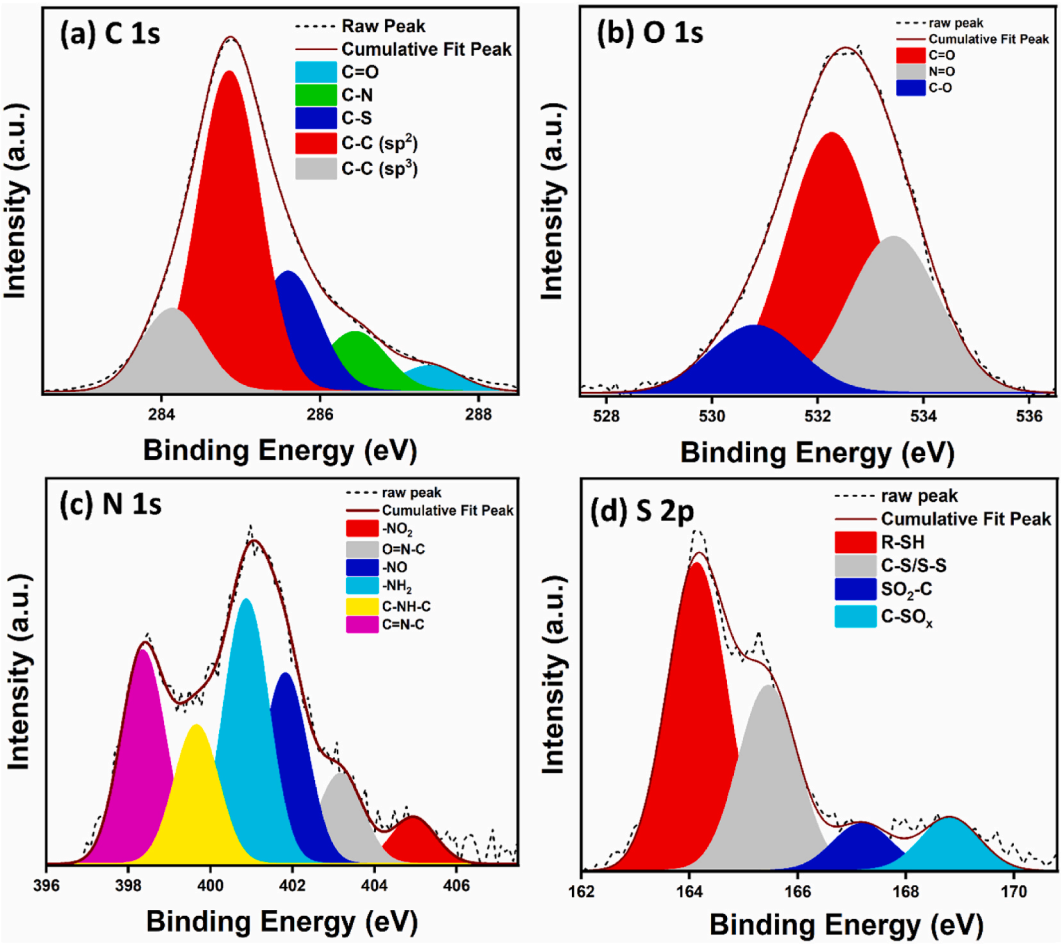

Fig. 4. XPS deconvoluted spectra of **(a)** C 1s, **(b)** O 1s, **(c)** N 1s, and **(d)** S 2p of mesoporous nanocarbon.

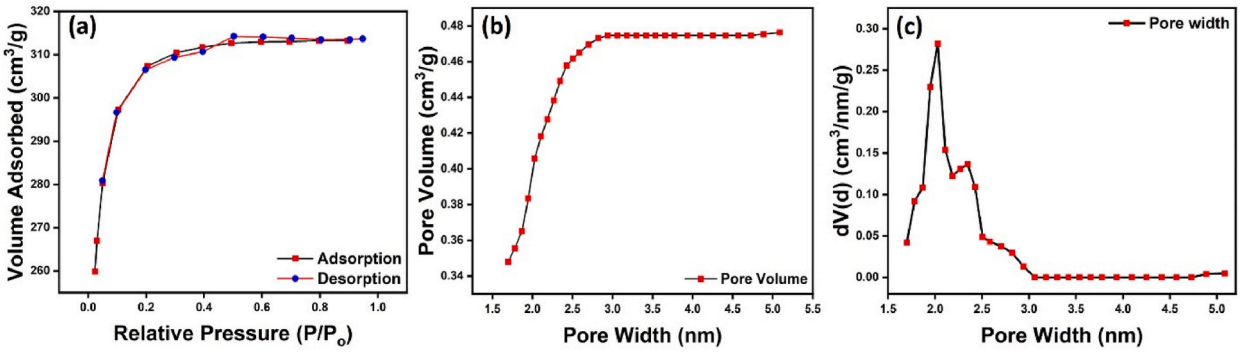

Fig. 5. **(a)** Adsorption-desorption isotherm, **(b)** pore volume and **(c)** pore width spectra of mesoporous nanocarbon.

The diffusion coefficient calculated from the equation for 10 mM $K_3[Fe(CN)_6]/K_4[Fe(CN)_6]$ in 0.1 M KCl is 2.1×10^{-6} cm^2/s. The obtained electroactive surface area of N, S-rich modified electrode after applying equation (1) is 0.35 cm^2. The relatively high electroactive surface area of N, S- nanocarbon modified electrode compared to the geometric surface of bare electrode was also added to the enhanced conductivity. Similarly, the scan rate study was done with 1 mM lead with modified GCE. A linear relationship with the observed current peak and scan rate also indicated a diffusion-controlled reaction mechanism of lead. The broadness of the peak with increasing scan rate also indicates a diffusion-controlled reaction. The calculated value of the diffusion coefficient after applying equation (1) for a lead solution is 7.5×10^{-6} cm^2/s.

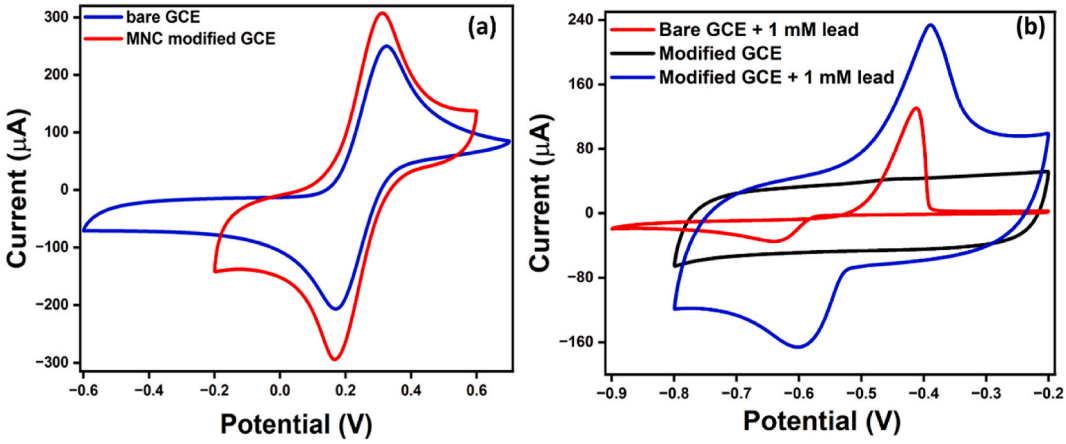

Fig. 6. Cyclic voltammogram of bare and mesoporous nanocarbon-modified GCE in the presence of **(a)** 10 mM $K_3[Fe(CN)_6]/K_4[Fe(CN)_6]$ in 0.1 M KCl and **(b)** 1 mM lead.

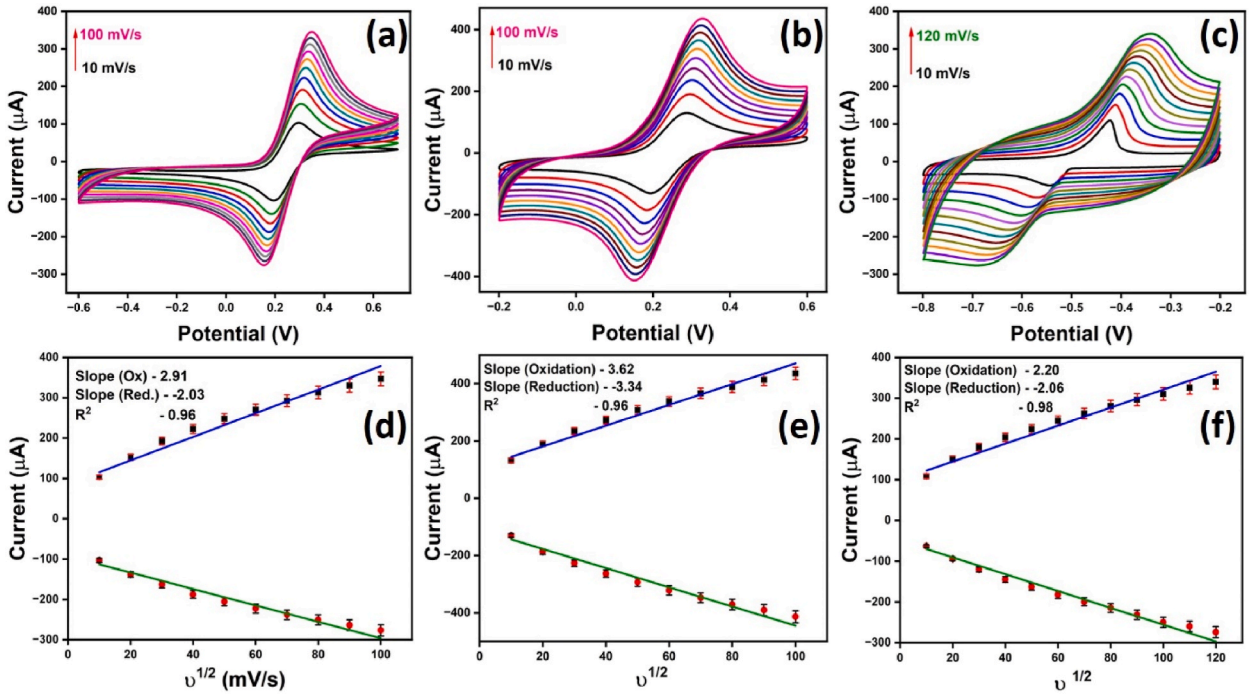

Fig. 7. Cyclic voltammogram of **(a)** bare and **(b)** mesoporous nanocarbon-modified GCE in the presence of 10 mM $K_3[Fe(CN)_6]/K_4[Fe(CN)_6]$ in 0.1 M KCl **(c)** 1 mM lead with mesoporous nanocarbon modified GCE at the scan rate ranging from 10 to 100 mV/s respectively and **(d–f)** respective linear relationship of oxidation and reduction peak current of corresponding to the above graph.

3.2.2. Differential pulse anodic stripping voltammetry

Differential pulse anodic stripping voltammetry (DPASV) is one of the highly sensitive techniques known for its high selectivity and quantification of trace metal ions. For the sensing of lead ions, the DPASV study was conducted, where the current of different lead concentrations were recorded. Fig. 8(a) shows the respective current response of N, S- rich nanocarbon modified electrode in the 60–140 nM range. Fig. 8(b) displays the observed linear relationship between the recorded current and associated concentration. The obtained detection limit after applying equation (2) is 0.022 μM. The obtained limit of quantification and sensitivity after using equations (3) and (4) is 0.075 μM and 0.11 nM/μA cm^2. The achievement of excellent detection limit can be due to high specific surface area, and presence of nitrogen and sulfur functional group on to the carbon substrate. A comparison of DPASV techniques with differential pulse normal voltammetry (DPNV) was studied, and a DPNV study was also conducted for sensing lead. Fig. S2 shows the DPNV curve of lead at the oxidation potential −0.4 V. The study has shown that the current peak increased linearly in the 50–200 μM concentration range. The detection limit of MNC obtained from this technique is 50.67 μM, which is relatively high compared to the

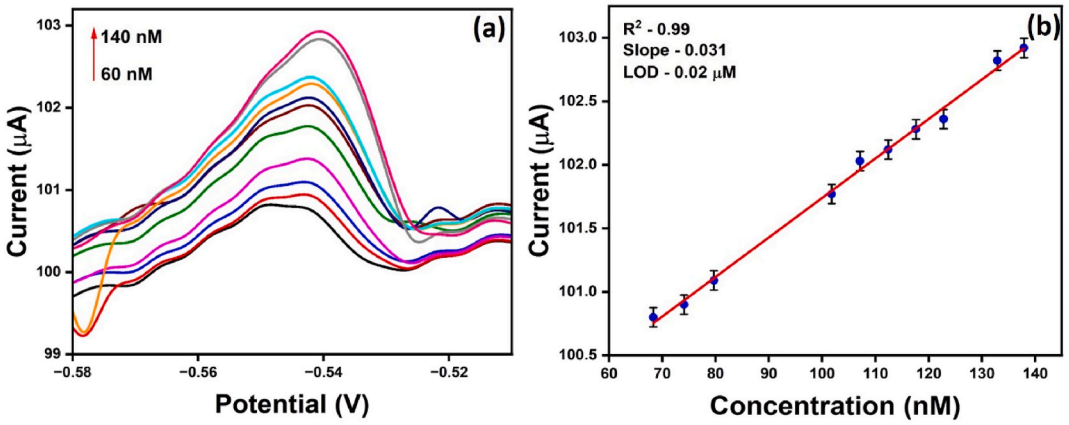

Fig. 8. **(a)** Differential pulse anodic stripping voltammogram of N, S-nanocarbon modified GCE recorded with different concentrations of lead 60–140 nM in acetate buffer and **(b)** linear relationship of current and concentration in the range 60–140 nM.

DPASV technique. It has been concluded that DPASV is a highly sensitive technique that can detect lead at the nanomolar level. Table 1 has added all the previously used nanoparticles to detect lead.

$$LOD = 3\sigma/S \tag{2}$$

$$LOQ = 10\sigma/S \tag{3}$$

$$Sensitivity = Slope/Area \tag{4}$$

3.3. Selectivity study

Selectivity study is one of the critical parameters to test the overall performance and affinity of as-synthesized nanocomposite. It is also helpful in selecting analytes based on the sensitivity of the modified electrode. The study was conducted in the presence of different metal ions (Ca^{2+}, K^{+}, Cd^{2+}, Fe^{2+}, Ag^{+}, Ni^{2+}, Fe^{3+}, Al^{3+}, Pb^{2+}, Co^{2+}, Na^{+}, and Hg^{2+}) 1 mM in 0.1 M acetate buffer electrolyte solution. Fig. 9(a) has displayed the current response of N, S- rich nanocarbon GCE, wherein the potential window of −1.5 to 1.5 V,

Table 1
Comparative response of different nanomaterials previously used for the detection of lead with reference to their detection methods, linear detection range, pH, detection limit, LOQ and sensitivity.

S. No.	Nanomaterial	Detection Method	Linear Detection Range	pH	Detection Limit	LOQ	Sensitivity	Ref.
1	1-dodecanoyl-3-phenylthiourea modified GCE	SWASV	100–1000 μM	3	0.695 μg/L	–	–	[43]
2	MWCNT-βCD(Phys)/SPE MWCNT-βCD(SE)/SPE	DPV	0.015–0.5 μM 6.2–103.5 ppb	5	0.9 ppb 2.3 ppb	–	98 nA/ppb 38.6 nA/ppb	[44]
3	Cu-based Sensor	ASV	0.025–10 μM	5.5	21 nM	–	–	[45]
4	PPy NPs	DPV	0.1–50 μM	5	55 nM	–	–	[46]
5	GR-5/$(Fe\text{-}P)_n$-MOF	CA	0–200 nM	5.5	0.034 nM	–	–	[2]
6	NHAP/Ionophore/Nafion-Modified Electrode	ASDPV	0.005–0.8 μM	4.4	1 nM	–	13 μA/μM	[47]
7	ZYMCPE	CV	0.0025–0.1 μM	5.9	17 nM	–		[48]
8.	GO-Fc	CV	0.1–1000 μg/L	–	0.168 μg/L	–	250 μg/L	[49]
9.	IP/NPs	DPSV	0.1–10 nM	5	30 pM	–	49.179 nA/nM	[13]
10.	Fe_3O_4@SiO_2@IIP	DPV	0.1–80 ng/mL	5.6	0.05 ng/mL	0.16 ng/mL	7962 μA/μmol dm^{-3}	[50]
11.	porph@MOF	SWV	50 pM −5 μM	–	5 pM	–	–	[1]
12.	Pb^{2+}-specific DNAzyme-based sensor	SWV	0.05–50 nM	4.3	32 pM	–	–	[3]
13.	G/PANI/PS	ASV	10–500 μg/L	1	3.30 μg/L	–	–	[51]
14.	MWCNT-IIP	DPV	1–5 ppm	5	0.02 μM	–	–	[52]
15.	MIP	DPV	0.3–50 μM	–	0.2 μM	–	–	[14]
16.	MWCNTs/GNP	DPV	5×10^{-11}-1×10^{-14} M	–	4.3 fM	–	–	[4]
17.	GO-imi-$(CH_2)_2$-NH_2)	DPASV	5–300 nM	5	0.30 nM	–	–	[53]
18.	N, S-rich nanocarbon	DPASV	60–140 nM	5	22 nM	75 nM	0.00011 μA/μM cm^2	This work

only four metal ions (Cd^{2+}, Pb^{2+}, Cu^{2+} and Hg^{2+}) has displayed the current response, where the peaks are distinguished. The current reaction of lead is higher among all the heavy metal ions. This has shown the high selectivity and affinity of as-synthesized nano sensors toward lead. Consequently, the current response was also recorded after varying the concentration of metal ions in acetate buffer (Fig. 9(b)) and tap water (Fig. 9(c)). It is well confirmed from the recorded results that an N, S-rich nanocarbon-modified electrode is highly efficient in detecting lead in the mixed metal component, even at low concentrations. Moreover, the modified electrode has also detected lead in the tap water mixture. This indicates that the as-synthesized nanocomposite is highly sensitive and selective toward lead in diverse environments and can be applied in real-time sensing.

3.4. Real sample-based sensing

To determine the reliability of the N, S-rich nanocarbon-modified electrode, the current response of lead in acetate buffer and tap water at varied concentrations is compared. Fig. 10(a) and Fig. 10(b) have shown the current response of varied concentrations of lead ions in different solutions. Although both graphs show a linear current response with respective concentrations, the current response of lead in tap water is relatively less. The bar graph in Fig. 10(c) shows the difference in current response at specific lead concentrations. The difference in current response can be due to the solubility issue of lead in tap water.

Although the difference in current response is minute, this can interfere with sensing accuracy in real time. In this case, lead calibration in different water sources can be successful before sensing an unknown concentration in an actual application.

3.5. Repeatability, reproducibility and stability study

The reliability and performance of the sensor can also be tested through repeatability, reproducibility, and stability studies. In the repeatability study, the current response of 1 mM lead was repeated under the same experimental conditions, while in the reproducibility study, the whole experiment, viz., solution and modification of electrode, is repeated. Fig. 11(a) shows the 50 cycles of CV with 1 mM lead, where the stable current response indicates the stability of N, S-rich nanocarbon-modified electrodes. Fig. 11(b) shows the current response of 1 mM lead after repetition of the experiment; the relative standard deviation calculated from the current response of 5 studies was 9.45 %. Fig. 11(c) represents the current response of N, S-rich nanocarbon after its storage in a room environment. The current response was recorded after interval periods of 7 days, where no significant change in the current response is recorded.

4. Conclusion

This study has explored the cheap and sustainable waste management approach, where coconut husk waste was treated and converted into nitrogen and sulfur-rich mesoporous carbon nanomaterials. All the characterization studies have indicated that graphene-like thin and transparent layers with the nonuniform scattering of the quantum dot-like structure were well developed with a high surface area of 1671.93 m^2/g along with pore width and pore volume of 2.02 nm and 0.476 cm^3/g, respectively. The diversity of nitrogen and sulfur functional groups in the carbon matrix has indicated the chemically active site for facilitating electron transfer and sensing of lead ions. The as-synthesized nanostructure was applied to the surface of the glassy carbon electrode, and the modified electrode was then used as a sensor for efficient detection of lead. The nitrogen and sulfur enrichment of the carbon matrix makes the nanostructure highly sensitive toward lead, while the morphological geometry aids in increasing the conductivity. The obtained detection limit, the limit of quantification and sensitivity were 22 nM, 75 nM, and 0.00011 $\mu A/\mu M\ cm^2$, respectively. Moreover, the as-prepared nanostructure also shows high selectivity toward lead, even in the presence of other metal ions in distilled or real water samples. The as-prepared nanomaterial has achieved the very low detection limit, showing its high efficiency and performance over costly metal-based nanoparticles.

CRediT authorship contribution statement

Ritika Sharma: Writing – original draft, Formal analysis, Data curation. **Dharmender Singh Rana:** Writing – original draft, Formal analysis, Data curation. **Abhishek Awasthi:** Formal analysis, Data curation. **Dilbag Singh:** Writing – review & editing, Formal analysis, Data curation. **Ahmed A. Ibrahim:** Formal analysis, Data curation. **Ahmad Umar:** Writing – review & editing, Data curation. **Sotirios Baskoutas:** Writing – review & editing, Data curation.

Ethical approval

This research did not involve human or animal samples.

Data availability

The datasets used and analyzed during the current study are available from the corresponding author on reasonable request.

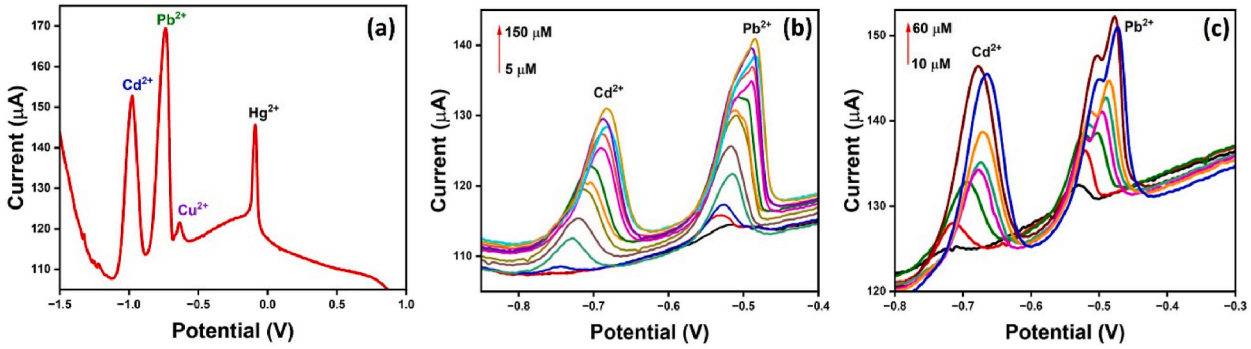

Fig. 9. **(a)** DPASV graph of N, S-nanocarbon in the presence of different metal ions viz., Ca, K^{+}, Cd^{2+}, Fe^{2+}, Ag^{+}, Ni^{2+}, Fe^{3+}, Al^{3+}, Pb^{2+}, Co^{2+}, Na^{+} and Hg^{2+} at a concentration **(a)** 1 mM **(b)** 5–150 μM in acetate buffer and **(c)** 10–60 μM in tap water.

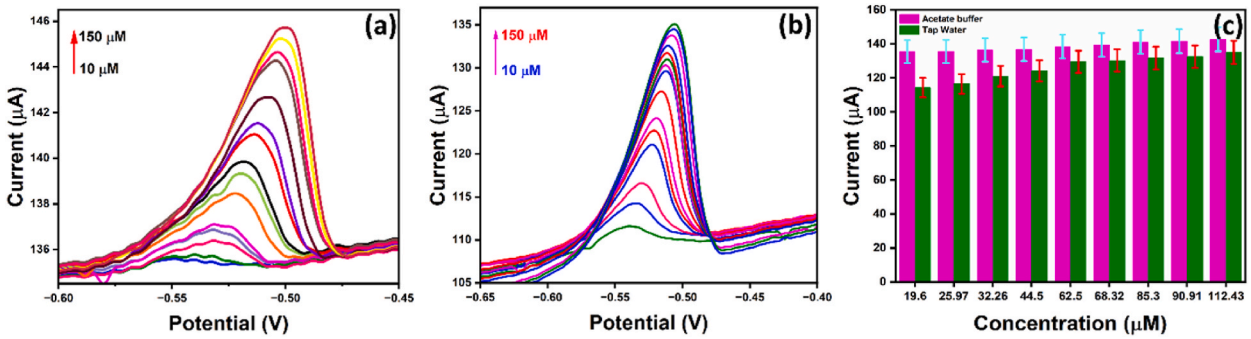

Fig. 10. DPASV response of N, S- nanocarbon modified GCE with the different concentrations of lead (10–150 μM) **(a)** in acetate buffer, **(b)** Tap water and **(c)** Bar graph showing a comparison of current response at the same concentration of lead in different solution viz., 0.1 M acetate buffer and tap water.

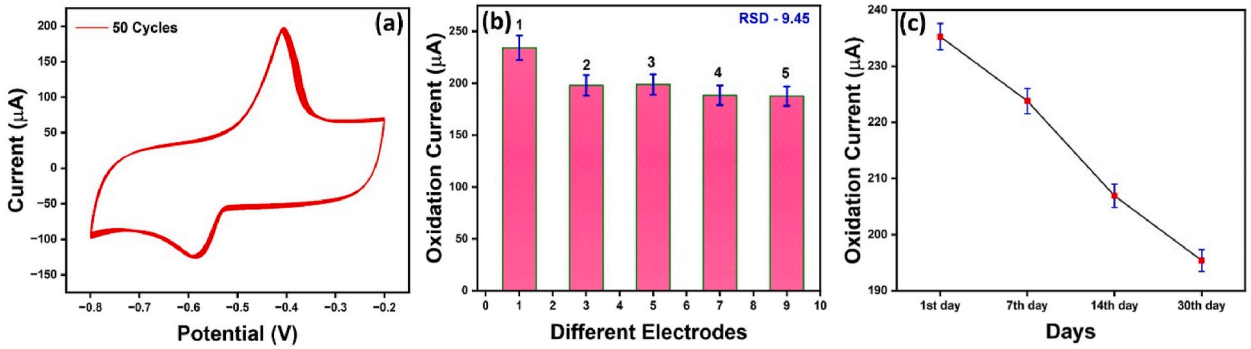

Fig. 11. Cyclic voltammetric response of 1 mM lead **(a)** 50 cycles, **(b)** with different N, S-nanocarbon modified GCE and **(c)** after successive intervals of 7 days of storage.

Declaration of competing interest

The authors declare that they have no known competing financial interests or personal relationships that could have appeared to influence the work reported in this paper.

Acknowledgment

RS is thankful to UGC-New Delhi for the award of SRF and Central University of Himachal Pradesh for providing necessary research facilities. Ahmad Umar and Ahmed A. Ibrahim would like to acknowledge the Research, Development and Innovation Authority (RDIA), Saudi Arabia for granting and financially supporting the "STEM Pioneers Training Lab" at Najran University.

Appendix A. Supplementary data

Supplementary data to this article can be found online at https://doi.org/10.1016/j.heliyon.2024.e39090.

References

[1] X. Zhang, X. Huang, Y. Xu, X. Wang, Z. Guo, X. Huang, Z. Li, J. Shi, X. Zou, Single-step electrochemical sensing of ppt-level lead in leaf vegetables based on peroxidase-mimicking metal-organic framework, Biosens. Bioelectron. 168 (2020) 112544, https://doi.org/10.1016/j.bios.2020.112544.

[2] T.P. Kamble, S.R. Shingte, V.D. Chavan, D.K. Kim, A.D. Chougale, T.D. Dongale, P.B. Patil, MOF derived $CoFe_2O_4$@Carbon nanofibers for supercapacitor application, ChemSci Adv. 1 (1) (2024) 34–40, https://doi.org/10.69626/csa.2024.0034.

[3] P. Pandey, S. Yadav, D.K. Dwivedi, P. Lohia, Development and modelling of a photonic crystal fiber sensor for detecting harmful chemicals in polycarbonate plastics, MatSci Express 1 (4) (2024) 253–261, https://doi.org/10.69626/mse.2024.0253.

[4] Y. Zhu, G. Zeng, Y. Zhang, L. Tang, J. Chen, M. Cheng, L. Zhang, L. He, Y. Guo, X. He, M. Lai, Y. He, Highly sensitive electrochemical sensor using a MWCNTs/GNPs-modified electrode for lead (II) detection based on Pb^{2+}-induced G-rich DNA conformation, Analyst 139 (19) (2014) 5014–5020, https://doi.org/10.1039/C4AN00874J.

[5] V. Mourya, S. Yadav, D.K. Dwivedi, P. Lohia, Design and evaluation of a twin-core photonic crystal fiber sensor for human blood biomolecules, SciEngg Adv. 1 (1) (2024) 20–29, https://doi.org/10.69626/sea.2024.0020.

[6] R.S. Salunke, Y. Nakate, A. Umar, A.M. Patil, U. Nakate, S. Baskoutas, D.J. Shirale, Selective recognition of lead and cadmium in potable water using single polypyrrole nanowire decorated with cobalt oxide nanoparticles electrode, MatSci Express 1 (2) (2024) 69–80, https://doi.org/10.69626/mse.2024.0069.

[7] T.R. Bhosale, S.B. Wategaonkar, P.P. Patil, P.V. Anbhule, M.B. Deshmukh, Crown ether functionalized barbituric acid for colorimetric determination of Au^{3+}, ChemSci Adv. 1 (3) (2024) 147–154, https://doi.org/10.69626/csa.2024.0147.

[8] V. Mariyappan, S. Manavalan, S.-M. Chen, G. Jaysiva, P. Veerakumar, M. Keerthi, Sr@FeNi-S nanoparticle/carbon nanotube nanocomposite with superior electrocatalytic activity for electrochemical detection of toxic mercury(II), ACS Appl. Electron. Mater. 2 (7) (2020) 1943–1952, https://doi.org/10.1021/acsaelm.0c00248.

[9] A.S. Ganie, S. Hussain, S. Shah, M.J. Liaqat, A.N. Begi, Z. Miao, Y. Han, In_2O_3 doped ZnO nanosheets for ultra-trace detection of NO_2, SciEngg Adv. 1 (2) (2024) 56–65, https://doi.org/10.69626/sea.2024.0056.

[10] S.K. Pawar, N.A. Wadodkar, R.S. Salunke, A.M. Patil, D.J. Shirale, Eco-friendly electrochemical sensor for accurate soil nitrate detection using ZnOx/PANI nanocomposite on nickel foam electrode, MatSci Express 1 (3) (2024) 170–178, https://doi.org/10.69626/mse.2024.0170.

[11] R. Sharma, S. Kumar, D.S. Rana, S. Thakur, N. Gupta, D. Singh, Molybdenum disulfide nanostructure grown on multi-walled carbon nanotube for the electrochemical detection of ofloxacin, J. Environ. Chem. Eng. 12 (2) (2024) 112413, https://doi.org/10.1016/j.jece.2024.112413.

[12] D.S. Rana, R. Sharma, S. Kumar, N. Gupta, S. Thakur, K.K. Thakur, D. Singh, Molybdenum disulfide (MoS_2) and reduced graphene oxide (rGO) nanocomposite based electrochemical sensor for detecting mercury(II) ions, Nano-Struct. Nano-Objects 36 (2023) 101041, https://doi.org/10.1016/j.nanoso.2023.101041.

[13] M.K. Bojdi, M.H. Mashhadizadeh, M. Behbahani, A. Farahani, S.S.H. Davarani, A. Bagheri, Synthesis, characterization and application of novel lead imprinted polymer nanoparticles as a high selective electrochemical sensor for ultra-trace determination of lead ions in complex matrixes, Electrochim. Acta 136 (2014) 59–65, https://doi.org/10.1016/j.electacta.2014.05.095.

[14] Z. Wang, Y. Qin, C. Wang, L. Sun, X. Lu, X. Lu, Preparation of electrochemical sensor for lead(II) based on molecularly imprinted film, Appl. Surf. Sci. 258 (6) (2012) 2017–2021, https://doi.org/10.1016/j.apsusc.2011.05.005.

[15] A. Soni, R. Sharma, D.S. Rana, D. Singh, N. Gupta, Structural designs of functional metal organic frameworks for the detection of mercury in contaminated water sources, Coord. Chem. Rev. 494 (2023) 215343, https://doi.org/10.1016/j.ccr.2023.215343.

[16] R. Sharma, D.S. Rana, N. Gupta, S. Thakur, K.K. Thakur, D. Singh, *Parthenium hysterophorus* derived nanostructures as an efficient carbocatalyst for the electrochemical sensing of mercury(II) ions, Chemosphere 354 (2024) 141591, https://doi.org/10.1016/j.chemosphere.2024.141591.

[17] R. Gusain, N. Kumar, S.S. Ray, Recent advances in carbon nanomaterial-based adsorbents for water purification, Coord. Chem. Rev. 405 (2020) 213111, https://doi.org/10.1016/j.ccr.2019.213111.

[18] Sahil, S. Kumar, Y.B. Barot, R. Mishra, D. Singh, N. Gupta, Nitrogen-doped fluorescent active fullerenes as a fluorescent probe for the detection of Hg^{2+} ions in aqueous solutions, Environ. Nanotechnol. Monit. Manag. 20 (2023) 100845, https://doi.org/10.1016/j.enmm.2023.100845.

[19] S. Kumar, R. Sharma, D. Singh, A. Awasthi, V. Kumar, K. Singh, Tungsten sulphide decorated carbon nanotube based electroanalytical sensing of neurotransmitter dopamine, Electrochim. Acta 475 (2024) 143584, https://doi.org/10.1016/j.electacta.2023.143584.

[20] S. Kalia, R. Kumar, R. Sharma, S. Kumar, D. Singh, R.K. Singh, Two-dimensional layered rGO-MoS_2 heterostructures decorated with Fe_3O_4 nanoparticles as an electrochemical sensor for detection of para-nitrophenol, J. Phys. Chem. Solid. 184 (2024) 111719, https://doi.org/10.1016/j.jpcs.2023.111719.

[21] S. Kumar, D. Singh, D. Pathania, A. Awasthi, K. Singh, Molybdenum disulphide-nitrogen doped reduced graphene oxide heterostructure based electrochemical sensing of epinephrine, Mater. Chem. Phys. 297 (2023) 127446, https://doi.org/10.1016/j.matchemphys.2023.127446.

[22] D.S. Rana, S. Kalia, N. Thakur, R.K. Singh, R. Kumar, D. Singh, Synthesis of reduced graphene oxide-molybdenum disulfide nanocomposite as potential scaffold for fabrication of efficient hydrazine sensor, Mater. Chem. Phys. 294 (2023) 127048, https://doi.org/10.1016/j.matchemphys.2022.127048.

[23] R. Sharma, J. Thakur, V.B. Jaryal, D.S. Rana, S. Thakur, N. Gupta, D. Singh, Nitrogen and sulfur functionalized microporous carbon nanomaterial derived from waste coconut husk for the efficient detection and removal of ofloxacin, Chemosphere 346 (2024) 140653, https://doi.org/10.1016/j.chemosphere.2023.140653.

[24] N. Farooq, Z. Rehman, A. Hareem, R. Masood, R. Ashfaq, I. Fatimah, S. Hussain, S.A. Ansari, N. Parveen, Graphene oxide and based materials: synthesis, properties, and applications – a comprehensive review, MatSci Express 1 (4) (2024) 185–231, https://doi.org/10.69626/mse.2024.0185.

[25] D.S. Rana, R. Sharma, N. Gupta, V. Sharma, S. Thakur, D. Singh, Development of metal free carbon catalyst derived from parthenium hysterophorus for the electrochemical detection of dopamine, Environ. Res. 231 (2023) 116151, https://doi.org/10.1016/j.envres.2023.116151.

[26] L. Ji, B. Wang, Y. Yu, N. Wang, J.N. Zhao, S Co-doped biomass derived carbon with sheet-like microstructures for supercapacitors, Electrochim. Acta 331 (2020) 135348, https://doi.org/10.1016/j.electacta.2019.135348.

[27] N. Sreekanth, M.A. Nazrulla, T.V. Vineesh, K. Sailaja, K.L. Phani, Metal-free boron-doped graphene for selective electroreduction of carbon dioxide to formic acid/formate, Chem. Commun. 51 (89) (2015) 16061–16064, https://doi.org/10.1039/C5CC06051F.

[28] L. Zhang, J. Xiao, H. Wang, M. Shao, Carbon-based electrocatalysts for hydrogen and oxygen evolution reactions, ACS Catal. 7 (11) (2017) 7855–7865, https://doi.org/10.1021/acscatal.7b02718.

[29] K.S. Novoselov, A.K. Geim, S.V. Morozov, D. Jiang, Y. Zhang, S.V. Dubonos, I.V. Grigorieva, A.A. Firsov, Electric field effect in atomically thin carbon films, Science 306 (5696) (2004) 666–669, https://doi.org/10.1126/science.1102896.

[30] J. Deng, M. Li, Y. Wang, Biomass-derived carbon: synthesis and applications in energy storage and conversion, Green Chem. 18 (18) (2016) 4824–4854, https://doi.org/10.1039/C6GC01172A.

[31] Coconut Husk Waste-Derived Nitrogen-Doped Mesoporous Carbon Nanomaterial as an Efficient and Sustainable Supercapacitor - Sharma - 2024 - Energy Technology - Wiley Online Library. https://onlinelibrary.wiley.com/doi/abs/10.1002/ente.202400294 (accessed 2024-08-07).

[32] K.M. Zeinu, H. Hou, B. Liu, X. Yuan, L. Huang, X. Zhu, J. Hu, J. Yang, S. Liang, X. Wu, A novel hollow sphere bismuth oxide doped mesoporous carbon nanocomposite material derived from sustainable biomass for picomolar electrochemical detection of lead and cadmium, J. Mater. Chem. A 4 (36) (2016) 13967–13979, https://doi.org/10.1039/C6TA04881A.

[33] X. Zhu, B. Liu, S. Chen, L. Wu, J. Yang, S. Liang, K. Xiao, J. Hu, H. Hou, Ultrasensitive and simultaneous electrochemical determination of Pb2+ and Cd2+ based on biomass derived Lotus root-like hierarchical porous carbon/bismuth composite, J. Electrochem. Soc. 167 (8) (2020) 087505, https://doi.org/10.1149/1945-7111/ab82f7.
[34] X. Chen, K. Lu, D. Lin, Y. Li, S. Yin, Z. Zhang, M. Tang, G. Chen, Hierarchical porous tubular biochar based sensor for detection of trace lead (II), Electroanalysis 33 (2) (2021) 473–482, https://doi.org/10.1002/elan.202060148.
[35] Z. Zeng, S. Fang, D. Tang, R. Xiao, L. Tang, B. Peng, J. Gong, B. Long, X. Ouyang, G. Zeng, Ultrasensitive sensor based on novel bismuth carbon nanomaterial for lead and cadmium determination in natural water, contaminated soil and human plasma, Microporous Mesoporous Mater. 284 (2019) 177–185, https://doi.org/10.1016/j.micromeso.2019.04.045.
[36] D. Agustini, A.S. Mangrich, M.F. Bergamini, L.H. Marcolino-Junior, Sensitive voltammetric determination of lead released from ceramic dishes by using of bismuth nanostructures anchored on biochar, Talanta 142 (2015) 221–227, https://doi.org/10.1016/j.talanta.2015.04.052.
[37] H. Jin, D. Zhang, Y. Liu, M. Wei, An electrochemical aptasensor for lead ion detection based on catalytic hairpin assembly and porous carbon supported platinum as signal amplification, RSC Adv. 10 (11) (2020) 6647–6653, https://doi.org/10.1039/D0RA00022A.
[38] M. Dali, K. Zinoubi, A. Chrouda, S. Abderrahmane, S. Cherrad, N. Jaffrezic-Renault, A biosensor based on fungal soil biomass for electrochemical detection of lead (II) and cadmium (II) by differential pulse anodic stripping voltammetry, J. Electroanal. Chem. 813 (2018) 9–19, https://doi.org/10.1016/j.jelechem.2018.02.009.
[39] C. Xu, J. Liu, Y. Bi, C. Ma, J. Bai, Z. Hu, M. Zhou, Biomass derived worm-like nitrogen-doped-carbon framework for trace determination of toxic heavy metal lead (II), Anal. Chim. Acta 1116 (2020) 16–26, https://doi.org/10.1016/j.aca.2020.04.033.
[40] G.A. Oliveira, A. Gevaerd, A.S. Mangrich, L.H. Marcolino-Junior, M.F. Bergamini, Biochar obtained from spent coffee grounds: evaluation of adsorption properties and its application in a voltammetric sensor for lead (II) ions, Microchem. J. 165 (2021) 106114, https://doi.org/10.1016/j.microc.2021.106114.
[41] J. Guan, Y. Fang, T. Zhang, L. Wang, H. Zhu, M. Du, M. Zhang, Kelp-derived activated porous carbon for the detection of heavy metal ions via square wave anodic stripping voltammetry, Electrocatalysis 11 (1) (2020) 59–67, https://doi.org/10.1007/s12678-019-00568-9.
[42] N. Tripathi, C.D. Hills, R.S. Singh, C.J. Atkinson, Biomass waste utilisation in low-carbon products: harnessing a major potential resource, Npj Clim. Atmospheric Sci. 2 (1) (2019) 1–10, https://doi.org/10.1038/s41612-019-0093-5.
[43] A. Shah, A. Zahid, A. Khan, F.J. Iftikhar, J. Nisar, C. Fernandez, M.S. Akhter, A.A. Almutawah, H.-B. Kraatz, Development of a highly sensitive electrochemical sensing platform for the trace level detection of lead ions, J. Electrochem. Soc. 166 (9) (2019) B3136–B3142, https://doi.org/10.1149/2.0271909jes.
[44] A.U. Alam, M.M.R. Howlader, N.-X. Hu, M.J. Deen, Electrochemical sensing of lead in drinking water using β-cyclodextrin-modified MWCNTs, Sensor. Actuator. B Chem. 296 (2019) 126632, https://doi.org/10.1016/j.snb.2019.126632.
[45] W. Kang, X. Pei, C.A. Rusinek, A. Bange, E.N. Haynes, W.R. Heineman, I. Papautsky, Determination of lead with a copper-based electrochemical sensor, Anal. Chem. 89 (6) (2017) 3345–3352, https://doi.org/10.1021/acs.analchem.6b03894.
[46] T. Xu, H. Dai, Y. Jin, Electrochemical sensing of lead(II) by differential pulse voltammetry using conductive polypyrrole nanoparticles, Microchim. Acta 187 (1) (2019) 23, https://doi.org/10.1007/s00604-019-4027-z.
[47] D. Pan, Y. Wang, Z. Chen, T. Lou, W. Qin, Nanomaterial/ionophore-based electrode for anodic stripping voltammetric determination of lead: an electrochemical sensing platform toward heavy metals, Anal. Chem. 81 (12) (2009) 5088–5094, https://doi.org/10.1021/ac900417e.
[48] S. Senthilkumar, R. Saraswathi, Electrochemical sensing of cadmium and lead ions at zeolite-modified electrodes: optimization and field measurements, Sensor. Actuator. B Chem. 141 (1) (2009) 65–75, https://doi.org/10.1016/j.snb.2009.05.029.
[49] N. Ashwin Karthick, R. Thangappan, M. Arivanandhan, A. Gnanamani, R. Jayavel, A facile synthesis of ferrocene functionalized graphene oxide nanocomposite for electrochemical sensing of lead, J. Inorg. Organomet. Polym. Mater. 28 (3) (2018) 1021–1028, https://doi.org/10.1007/s10904-017-0744-0.
[50] Z. Dahaghin, P.A. Kilmartin, H.Z. Mousavi, Novel ion imprinted polymer electrochemical sensor for the selective detection of lead(II), Food Chem. 303 (2020) 125374, https://doi.org/10.1016/j.foodchem.2019.125374.
[51] N. Promphet, P. Rattanarat, R. Rangkupan, O. Chailapakul, N. Rodthongkum, An electrochemical sensor based on graphene/polyaniline/polystyrene nanoporous fibers modified electrode for simultaneous determination of lead and cadmium, Sensor. Actuator. B Chem. 207 (2015) 526–534, https://doi.org/10.1016/j.snb.2014.10.126.
[52] M. Sebastian, B. Mathew, Ion imprinting approach for the fabrication of an electrochemical sensor and sorbent for lead ions in real samples using modified multiwalled carbon nanotubes, J. Mater. Sci. 53 (5) (2018) 3557–3572, https://doi.org/10.1007/s10853-017-1787-x.
[53] M.A. Eshlaghi, E. Kowsari, A. Ehsani, B. Akbari-Adergani, M. Hekmati, Functionalized graphene oxide GO-[imi-$(CH_2)_2$-NH_2] as a high efficient material for electrochemical sensing of lead: synthesis surface and electrochemical characterization, J. Electroanal. Chem. 858 (2020) 113784, https://doi.org/10.1016/j.jelechem.2019.113784.